JOURNAL OF CATALYSIS 150, 234–242 (1994)

Microcalorimetric, ^{13}C NMR Spectroscopic, and Reaction Kinetic Studies of Silica- and L-Zeolite-Supported Platinum Catalysts for *n*-Hexane Conversion

S. B. Sharma, [1] P. Ouraipryvan, H. A. Nair, [2] P. Balaraman, T. W. Root, and J. A. Dumesic[3]

Department of Chemical Engineering, University of Wisconsin-Madison, Madison, WI 53706

Received March 14, 1994; revised July 25, 1994

Reaction kinetics measurements of *n*-hexane conversion over 4% Pt/SiO_2 and 1% Pt/K(Ba)–L catalysts were made at a pressure of 3 atm and temperatures from 698 to 750 K. The rates of benzene and methylcyclopentane formation decrease with time during reaction over Pt/SiO_2, while 1% Pt/K(Ba)–L does not deactivate significantly. Microcalorimetric measurements at 353 K show that the heat of carbon monoxide adsorption is the same on freshly reduced Pt/SiO_2 and Pt/K(Ba)–L catalysts; however, carbonaceous species that accumulate on Pt/SiO_2 during *n*-hexane conversion decrease the total number of adsorption sites and the number of sites that adsorb carbon monoxide strongly. The 1% Pt/K(Ba)–L catalyst retains the adsorptive properties of the freshly reduced catalyst. Nuclear magnetic resonance studies of ^{13}CO adsorption show that cluster-sized platinum particles are more resistant to deactivation by self-poisoning reactions than larger platinum particles. The greater catalyst stability and higher steady-state activity of L-zeolite-supported platinum catalysts may be attributed to the ability of L-zeolite to stabilize cluster-sized particles under reaction conditions. Differences in dehydrocyclization activity between catalysts may be related to differences in the number of strong adsorption sites that are present under reaction conditions. © 1994 Academic Press, Inc.

INTRODUCTION

Platinum particles supported on neutral or basic L-zeolites are highly active and selective for dehydrocyclization reactions of normal paraffins (e.g., 1–6). It has recently been reported that the initial dehydrocyclization activities of clean, silica-supported platinum catalysts are comparable to the initial activities of L-zeolite-supported platinum catalysts (7), while the rates of catalyst deactivation are considerably different between these two types of catalysts. Specifically, L-zeolite-supported platinum catalysts maintain the initial high activity at steady state, while silica-supported catalysts deactivate to a lower steady-state activity (8).

We have reported in a recent study that freshly reduced platinum particles supported in L-zeolite have similar properties for hydrogen and carbon monoxide adsorption as platinum supported on silica (8). Thus, it appears that the unusual catalytic properties of zeolite-supported platinum catalysts cannot be attributed to unique support-dependent adsorptive properties of platinum. Accordingly, differences in catalyst deactivation rates may be related to morphological differences between the two types of catalysts. Indeed, it has been observed that small Pt particles within the L-zeolite pore structure are more resistant to coke formation during *n*-hexane conversion than larger particles located on the external surface of the zeolite (9).

In the present study, we have attempted to probe the surface properties of silica- and L-zeolite-supported platinum catalysts that have been exposed to reaction conditions for *n*-hexane aromatization. The purpose of this study was to ascertain the chemical nature of adsorption sites that remain accessible after the catalysts have reached steady-state activity. We have employed heat-flow microcalorimetry, ^{13}C NMR spectroscopy and steady-state reaction kinetics measurements to study how adsorbed carbonaceous species deposited on the catalyst surface during *n*-hexane reforming reactions affect the adsorptive properties of platinum and alter *n*-hexane reaction selectivities.

EXPERIMENTAL

Microcalorimetric Studies

Microcalorimetric measurements of differential enthalpy changes of adsorption were conducted using a Tian–Calvet heat-flow microcalorimeter (10). The microcalorimeter consists of two heat-flux transducers (ITI Corporation, Del Mar, CA), located in a thermostated alumi-

[1] Present address: Mobil Research and Development Corp., Central Research Laboratory, P.O. Box 1025, Princeton, NJ 08540.

[2] Present address: Procter and Gamble Company, 5299 Spring Grove Ave., Cincinnati, OH 45217.

[3] To whom correspondence should be addressed.

0021-9517/94 $6.00

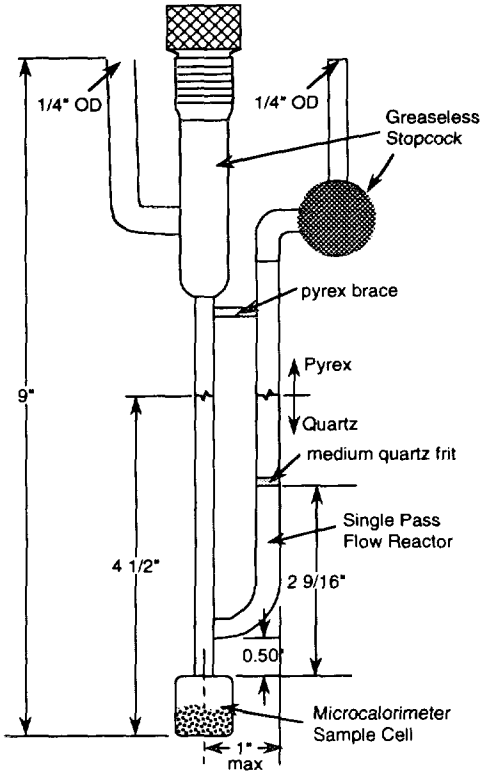

FIG. 1. Schematic diagram of cell for microcalorimetric measurements.

num block. One transducer holds a quartz sample cell, and the second transducer contains an empty cell that minimizes effects caused by fluctuations of the calorimeter temperature. The differential enthalpy change of adsorption is negative, and it is convenient to define the differential heat of adsorption as a positive quantity that is equal in magnitude to the differential enthalpy change.

A 4% Pt/SiO_2 catalyst and a 1% Pt/K(Ba)–L catalyst were used for microcalorimetric studies. The synthesis and treatment of these catalysts have been presented elsewhere (8). Prior to use, prereduced catalysts (ca. 500 mg) were treated in flowing hydrogen (ca. 100 cc/min) at 673 K for 2 h and subsequently degassed for 2 h at this temperature. Microcalorimetric measurements of carbon monoxide adsorption on reduced catalysts were then made at 353 K by sequentially dosing 1–3 μmol amounts of CO into the microcalorimetric cells until the platinum surface became saturated.

A schematic diagram of the quartz sample cell is shown in Fig. 1. This design permits the cell to be used for microcalorimetric measurements and for reaction kinetics studies, by inverting the cell and transferring the catalyst between the calorimetric compartment and the reactor section. The cell is fitted with greaseless stopcocks that permit the cell to be isolated and moved between the microcalorimetric apparatus and a reaction kinetics system without exposing the sample to the atmosphere.

Following microcalorimetric studies of reduced materials, the catalysts were treated for 2 h in a reaction mixture of hydrogen and *n*-hexane at 673 K and 1.5 atm. The reactor feed was maintained at a hydrogen : hexane ratio of 8 : 1 and a total gas flow rate of 500 cc/min. The *n*-hexane was then removed from the reactor feed, and the hydrogen flow was continued for 20 min, after which the sample cell was isolated in hydrogen and cooled to room temperature. The samples were degassed for 2 h at 473 K to remove adsorbed hydrogen, and microcalorimetric measurements of CO adsorption were conducted at 353 K on these aged samples. This adsorption temperature was sufficiently high to achieve equilibration of CO with the catalyst and sufficiently low to minimize surface reactions between carbon monoxide and any hydrocarbon species remaining on the catalyst following exposure to the hydrogen : hexane reaction mixture.

^{13}C NMR Spectroscopy Measurements

A U-tube Pyrex reactor fitted with greaseless stopcocks was used for ^{13}C NMR experiments. The U-tube reactor was designed to connect to a reaction kinetics system, where the 4% Pt/SiO_2 and 1% Pt/K(Ba)–L catalysts were subjected to the same reaction treatments as detailed for the microcalorimetric measurements. Prior to ^{13}CO adsorption studies, the samples were degassed for 2 h at 473 K to remove adsorbed hydrogen. Isotopically labeled carbon monoxide (99% ^{13}C, Isotech) was dosed into the evacuated sample cell at room temperature and the system allowed to equilibrate for 1 h. Weakly adsorbed ^{13}CO was removed from the catalyst by evacuating the gas-phase carbon monoxide at room temperature. The evacuated cell was then back-filled with argon to minimize atmospheric contamination during the 2–4 days required for spectral acquisition.

All ^{13}C NMR experiments were recorded at 300 K with a Chemagnetics CMC-300 solid-state NMR spectrometer operating at 75.34 MHz. Spectra were obtained by Fourier transformation of spin echoes (90^*_x–τ–180^*_y–τ–acquire). All peaks are reported in parts per million (ppm) downfield from tetramethylsilane (TMS), using the carbonyl resonance of acetic acid at 178.4 ppm as a secondary reference. ^{13}C spin counts in fully relaxed spectra were typically within 5–10% of the values predicted from CO uptake measurements during sample preparation.

n-Hexane Reaction Kinetics Studies

Reaction kinetics studies were conducted of *n*-hexane conversion over the 4% Pt/SiO_2 and 1% Pt/K(Ba)–L catalysts at a total pressure of 3 atm and at temperatures from 698 to 750 K. To minimize possible effects of transport

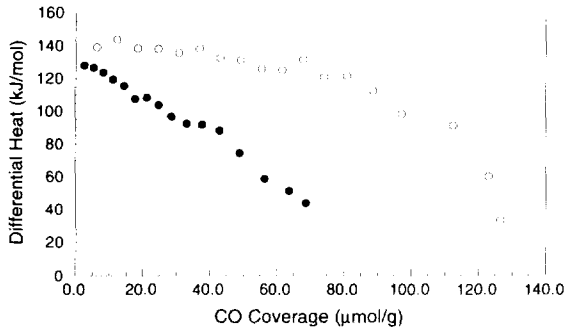

FIG. 2. Microcalorimetric results of carbon monoxide adsorption on 4% Pt/SiO_2 at 353 K. (○) Clean catalyst, (●) catalyst following *n*-hexane dehydrocyclization reaction.

limitations on the measured reaction kinetics, the Pt/K(Ba)–L catalyst was diluted by a factor of 10–15 with inactive K(Ba)–L zeolite. This dilution is necessary to minimize interparticle heat transfer limitations, which can create temperature gradients in the catalyst bed. The Pt/SiO_2 catalyst has a lower activity and does not suffer from similar heat transfer limitations. The amounts of catalyst used in these studies were adjusted to maintain the *n*-hexane conversion less than 12% at all reaction conditions.

Prior to reaction kinetics measurements, the 4% Pt/SiO_2 and 1% Pt/K(Ba)–L catalysts were reduced in flowing hydrogen at 773 K for 1–2 h. In addition, the Pt/SiO_2 catalyst was calcined at 573 K for 3–4 h in flowing oxygen prior to the reduction treatment. After the catalyst treatments, the reactor temperature was lowered to the desired temperature and the catalyst exposed to a reaction mixture of hydrogen and *n*-hexane. The reactor feed typically consisted of a hydrogen : hexane ratio of 10 : 1 at a total gas-flow rate of 500 cc/min. The reactor temperature and pressure were allowed to stabilize for 5–10 min before the first sample of the reactor effluent was collected for gas-chromatographic analysis. The hexane isomers, benzene, and C_5–C_3 hydrocarbons were separated on a 24-ft DC200 column. To minimize analysis times, methane and ethane were not separated from hydrogen and are not reported in the data. The reactor effluent was sampled every 25 min for up to 4 h. A fresh quantity of catalyst was used at each reaction condition to avoid possible contributions from catalyst deactivation to the observed reaction kinetics.

RESULTS

Microcalorimetric Studies

Microcalorimetric results of carbon monoxide adsorption at 353 K on freshly reduced and aged Pt/SiO_2 are shown in Fig. 2. The initial heat of adsorption for the aged catalyst is similar to the value measured for the clean sample. The heat of adsorption, however, decreases more rapidly with increasing carbon monoxide coverage for the aged catalyst. The total number of sites that are capable of adsorbing carbon monoxide is decreased by approximately 50% following exposure to the hydrogen : hexane reaction mixture. A similar loss of accessible platinum adsorption sites has been reported for platinum supported on γ-alumina following reactions involving *n*-hexane (11). Figure 2 also shows that only about 10% of the adsorption sites continue to bind carbon monoxide strongly on the aged catalyst. Subsequent calcination and reduction of the aged catalyst restores the adsorption characteristics of the initially clean catalyst for CO adsorption. Consequently, the loss of adsorption sites and decrease in the heat of CO adsorption are a result of carbonaceous species on the platinum surface.

Microcalorimetric results of carbon monoxide adsorption on initially clean and aged Pt/K(Ba)–L are shown in Fig. 3. Unlike the silica-supported sample, the aged Pt/K(Ba)–L catalyst retains most of the adsorption capacity of the clean sample. Furthermore, the data in Fig. 3 show that the aged catalyst retains the strong adsorption sites characteristic of clean platinum. These results suggest that negligible amounts of strongly bound carbonaceous species remain on the L-zeolite-supported platinum particles following exposure to the hydrogen : hexane reaction mixture.

^{13}C NMR Spectroscopy Measurements

The ^{13}C NMR spectrum of isotopically labeled carbon monoxide on aged Pt/SiO_2 is compared in Fig. 4 with the corresponding spectrum of the initially clean sample. The sharp ^{13}C signals at ca. 25 and 127 ppm observed for the aged sample result from sp^3- and sp^2-hybridized carbon atoms, respectively, deposited on the catalyst during reaction. It is apparent from this spectrum that the quantity of carbonaceous material deposited is ~100 times greater

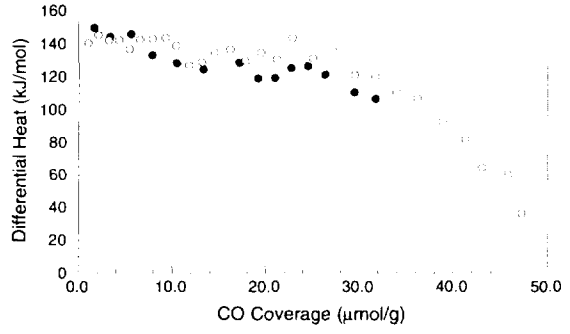

FIG. 3. Microcalorimetric results of carbon monoxide adsorption on 1% Pt/K(Ba)L-zeolite at 353 K. (○) Clean catalyst, (●) catalyst following *n*-hexane dehydrocyclization reaction.

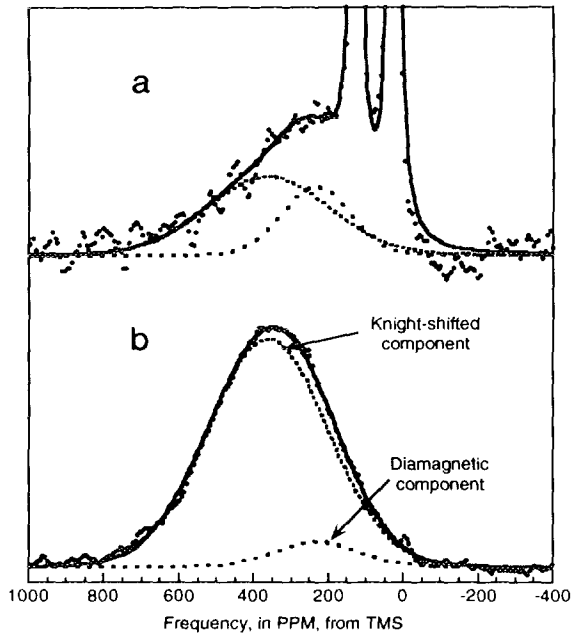

FIG. 4. (a) ^{13}C NMR spectrum of ^{13}CO adsorbed on 4% Pt/SiO_2 following *n*-hexane reforming reaction. (b) ^{13}C NMR spectrum of ^{13}CO adsorbed on reduced 4% Pt/SiO_2, taken from Ref. (12). Spectral deconvolution results are also shown.

than the amount of CO that can be subsequently adsorbed on the Pt particles (since ^{13}C is only present at 1.1% natural abundance in the hexane reactant). A significant fraction of this carbon is unsaturated (i.e., showing sp^2 hybridization). In addition, the carbon deposits have significant mobility, since narrow lines are observed without employing spinning or dipolar decoupling techniques. These observations suggest that the carbonaceous deposits are likely to be oligomers with substantial chain mobility that can migrate from the Pt particles to the support.

Contributions from isotopically labeled carbon monoxide adsorbed on the aged and the initially clean Pt/SiO_2 catalysts result in the broad band at higher chemical shift values. The contributions from different types of adsorbed species were deconvoluted by a computer fit of the overall spectrum (12). The results from this procedure are plotted in Fig. 4. This analysis indicates that the NMR spectra consist of (i) contributions centered at 210 ppm from ^{13}CO adsorbed on cluster-sized, diamagnetic platinum particles, and (ii) broad, Knight-shifted contributions centered at 360 ppm from ^{13}CO adsorbed on larger platinum particles. These assignments of diamagnetic and Knight-shifted contributions are described in detail elsewhere (12).

Comparison of Figs. 4a and 4b shows that the relative contribution of the diamagnetic component to the overall spectrum increases for the aged catalyst, causing a decrease in the mean chemical shift of the spectrum. Table 1 presents the ^{13}C spin counts for diamagnetic and Knight-shifted CO on Pt/SiO_2, showing that exposure of the catalyst to the hydrogen : hexane reaction mixture results in the selective loss of CO adsorption sites on the larger platinum particles. Specifically, the contribution from Knight-shifted CO decreases, while the amount of diamagnetic CO on small clusters remains essentially unchanged.

TABLE 1

^{13}C Spin Counts for CO on Pt/SiO_2

Species	Clean sample (μmol/g)	After reaction (μmol/g)	Sites lost (%)
Knight-shifted CO (large Pt particles)	79	26	67
Diamagnetic Co (small Pt clusters)	20	19	5
Total CO (exposed Pt sites)	99	45	55

n-Hexane Reaction Kinetics Studies

The Pt/K(Ba)–L catalyst maintained its initial catalytic activity for at least 4 h, which was the duration of the present kinetics experiments. The activity of the Pt/SiO_2 catalyst, however, decreased by nearly an order of magnitude during the first 30 min of exposure to the reaction mixture. The overall extent of catalyst deactivation for the silica-supported catalyst increased with increasing reaction temperature and decreasing hydrogen pressure. The kinetic data reported in this paper were collected after both catalysts had reached steady-state activity, generally requiring 1 h under reaction conditions.

Table 2 summarizes the product distributions observed over each catalyst at 698 K. Product yield is defined in

TABLE 2

Product Yield for *n*-Hexane Conversion at 698 K and P_{H_2} = 276 kPa, $P_{C_6H_{14}}$ = 27.6 kPa

Reaction	1% Pt/K(Ba)–L (%)	4% Pt/SiO_2 (%)
Dehydrocyclization[a]	72	27
Isomerization[b]	19	56
Hydrogenolysis[c]	9	16

[a] Yield defined as mole of Benzene + MCP produced/moles *n*-hexane converted.

[b] Yield defined as mole of 2MP + 3MP produced/moles *n*-hexane converted.

[c] Yield defined as mole of $C_5 + C_4 + C_3$ produced/moles *n*-hexane converted.

TABLE 3

Turnover Frequencies (sec^{-1}) for *n*-Hexane Conversion at 698 K and P_{H_2} = 276 kPa, $P_{C_6H_{14}}$ = 27.6 kPa

Component	1% Pt/K(Ba)–L	4% Pt/SiO_2
n-Hexane	1.2	0.19
Benzene	0.58	0.016
Methylcyclopentane	0.25	0.037
2-Methylpentane	0.12	0.071
3-Methylpentane	0.099	0.039
n-Pentane	0.034	0.0088
n-Butane	0.029	0.012
n-Propane	0.034	0.011

Table 2 as moles of product produced per mole of *n*-hexane converted. Dehydrocyclization and isomerization processes are the major reactions observed over both catalysts, with a smaller contribution from hydrogenolysis reactions to the product distribution. At the hydrogen partial pressures used in this study, olefin products are thermodynamically limited to less than 0.5% of the alkane components and are equilibrated at all reaction temperatures.

The steady-state rates of formation of the different products at the indicated reaction conditions are reported in Table 3. The turnover frequencies listed in Table 3 were calculated based on the numbers of surface Pt atoms for the clean catalysts, as determined by hydrogen chemisorption (8). The 1% Pt/K(Ba)–L catalyst is an order of magnitude more active for the formation of benzene and methylcyclopentane than the 4% Pt/SiO_2 catalyst. Both catalysts exhibit low activity for hydrogenolysis reactions. These results are in agreement with data obtained collected over similar catalysts by Lane *et al.* (13), Mielczarski *et al.* (14), and Ostgard *et al.* (9) for *n*-hexane reforming reactions, and by Iglesia and Baumgartner (7) for *n*-heptane reforming reactions.

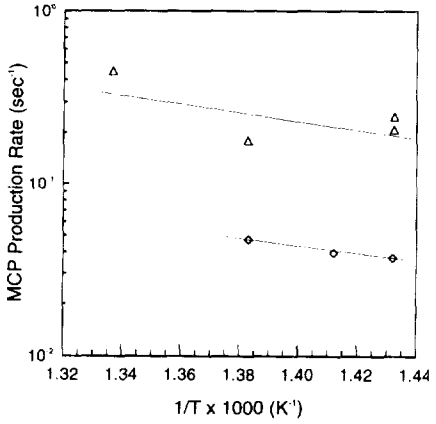

FIG. 6. Arrhenius plot for *n*-hexane dehydrocyclization to methylcyclopentane at P_{H_2} = 276 kPa, $P_{C_6H_{14}}$ = 27.6 kPa, 9–12% conversion over (△) 1% Pt/K(Ba)–L and (◇) 4% Pt/SiO_2.

The Pt/K(Ba)–L catalyst displays higher selectivity for terminal cracking than the Pt/SiO_2 catalyst. In particular, *n*-pentane/*n*-butane ratio is 1.2 over Pt/K(Ba)–L and 0.76 over Pt/SiO_2. The value of this ratio over Pt/K(Ba)–L is not as high as that reported by Tauster and Steger (15, 16) for similar catalysts. This difference may be due to the higher conversions of our study, which would result in increased contributions from secondary hydrogenolysis reactions. The *n*-pentane/*n*-butane ratio is less than unity for the silica-supported catalyst, and this result is in agreement with values reported for similar catalysts by these authors.

Arrhenius plots for the primary reactions of *n*-hexane

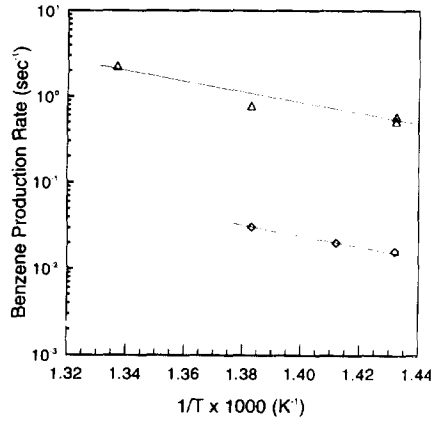

FIG. 5. Arrhenius plot for *n*-hexane dehydrocyclization to benzene at P_{H_2} = 276 kPa, $P_{C_6H_{14}}$ = 27.6 kPa, 9–12% conversion over (△) 1% Pt/K(Ba)–L and (◇) 4% Pt/SiO_2.

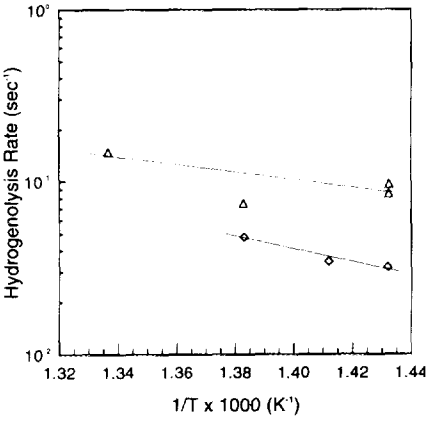

FIG. 7. Arrhenius plot for *n*-hexane hydrogenolysis to *n*-pentane and *n*-butane at P_{H_2} = 276 kPa, $P_{C_6H_{14}}$ = 27.6 kPa, 9–12% conversion over (△) 1% Pt/K(Ba)–L and (◇) 4% Pt/SiO_2.

TABLE 4

Apparent Activation Energies for *n*-Hexane Conversion at P_{H_2} = 276 kPa, $P_{C_6H_{14}}$ = 27.6 kPa

Production reaction	1% Pt/K(Ba)–L (kcal/mol)	4% Pt/SiO_2 (kcal/mol)
Benzene	28	26
Methylcyclopentane	12	10
n-Pentane	20	17
n-Butane	15	17

over the Pt/K(Ba)–L and Pt/SiO_2 catalysts are shown in Figs. 5–7, and the calculated values of the apparent activation energies are summarized in Table 4. Similar values for the apparent activation energies are obtained over both catalysts, suggesting that similar reaction mechanisms may be responsible for product formation. The values of the apparent activation energies are in agreement with those reported by Somorjai and co-workers for *n*-hexane aromatization over platinum single-crystal surfaces [17].

The dependence of the reaction rates on hydrogen pressure was investigated for the Pt/K(Ba)–L catalyst by varying the hydrogen partial pressure from ca. 270 to 370 Torr, while keeping the *n*-hexane pressure constant. The dehydrocyclization reaction rates show a negative dependence on the hydrogen partial pressure. Specifically, the hydrogen orders for benzene and methylcyclopentane production are −2.3 and −0.88, respectively. This behavior is characteristic of dehydrogenation reactions where hydrogen pressure has an inhibiting effect on the reaction rate (18). The hydrogen orders for the hydrogenolysis reactions producing *n*-pentane and *n*-butane are 1.08 and 1.28, respectively. It has been observed that hydrogen orders for alkane hydrogenolysis reactions exhibit maxima as the hydrogen partial pressure is increased (19). The pressure corresponding to this maximum increases with the size of the alkane, thereby extending the pressure range over which the hydrogenolysis reaction exhibits positive order.

DISCUSSION

Catalyst Deactivation

Loss of platinum surface area due to the accumulation of carbonaceous species during *n*-hexane conversion has been documented in the literature ((11, 20) and references therein). It is noteworthy that the 50% decrease in platinum surface area determined in the present study from microcalorimetric measurements of CO adsorption (Fig. 2) is in excellent agreement with the decrease in extent of CO adsorption determined by ^{13}C spin counts of NMR spectra (Table 1). This 50% decrease in platinum surface area, however, is not sufficient to explain the order of magnitude loss in catalytic activity observed for the Pt/SiO_2 catalyst. The microcalorimetric measurements indicate that most of the accessible adsorption sites on the aged Pt/SiO_2 catalyst bind carbon monoxide more weakly than the clean platinum surface. In agreement with these findings, temperature-programmed desorption spectra of carbon monoxide from platinum single-crystal surfaces deactivated during *n*-hexane reactions also show a decrease in the carbon monoxide desorption temperature from the clean surface (21). At present, we can not specify the detailed origin for the decrease in strength of CO adsorption on the sites remaining accessible on the Pt/SiO_2 catalyst following exposure to reaction conditions. For example, carbonaceous species may preferentially block strong adsorption sites or exposed Pt surface atoms adjacent to carbonaceous species may become weaker adsorption sites. A small fraction of the adsorption sites on the aged catalyst continues to bind carbon monoxide as strongly as the clean platinum catalyst. The extent of catalyst deactivation appears to scale with loss of strong CO adsorption sites. These results suggest that the strong adsorption sites may be related to the paraffin dehydrocyclization activity of the catalyst.

In contrast to the silica-supported catalyst, the Pt/K(Ba)–L catalyst retains essentially all of the platinum sites for CO adsorption following exposure of the catalyst to *n*-hexane reaction conditions. This result is consistent with the observation that the zeolite-supported catalyst does not deactivate significantly during reaction. Furthermore, the microcalorimetric data shown in Fig. 3 illustrate that the aged Pt/K(Ba)–L catalyst retains the strong carbon monoxide adsorption sites that appear to be important for catalytic activity. These results provide further support for the suggestion that the strong adsorption sites of platinum are necessary for dehydrocyclization activity of the catalyst.

We have previously reported that clean 1% Pt/K(Ba)–L and 4% Pt/SiO_2 catalysts have energetically similar sites for H_2 and CO adsorption (8). This conclusion is consistent with the observation of the present study and a previous study (7) that the initial activities of both catalysts are similar. The primary difference between these materials is the rate of catalyst deactivation. Carbonaceous species that accumulate on the silica-supported catalyst reduce the number of adsorption sites and selectively decrease the number of sites that strongly adsorb carbon monoxide. Accordingly, the unique catalytic properties of L-zeolite-supported platinum catalysts appear to be a consequence of their resistance to self-poisoning reactions that lead to the accumulation of adsorbed carbonaceous residue on the catalyst.

We further suggest that the resistance of L-zeolite-sup-

ported platinum catalysts to deactivation is related to the predominance of cluster-sized platinum particles that are stabilized in the L-zeolite structure. In particular, the resistance of cluster-sized platinum particles to self-poisoning reactions is seen for the Pt/SiO_2 catalyst by comparing the ^{13}C NMR spectra in Fig. 4 of carbon monoxide adsorbed on clean and aged samples. The contribution to the overall spectrum from ^{13}CO adsorbed on the cluster-sized, diamagnetic platinum particles is unchanged between the two spectra, while the contribution from the Knight-shifted ^{13}CO species on large platinum particles is reduced to about 35% of its former value on the aged catalyst. This result indicates that platinum particles large enough to exhibit a Knight-shifted resonance are selectively poisoned by carbonaceous species, compared to cluster-sized, diamagnetic particles. The carbonaceous material formed on these larger particles prevents CO adsorption on 53 μmol/g of Pt sites, either by direct bonding to the surface Pt or by physically occluding the surface without direct chemical interaction. Since hexane is substantially larger than CO, it may be expected that this carbonaceous overlayer will block an even larger proportion of the hexane reaction activity of these larger particles.

The resistance of small platinum particles to poisoning by carbonaceous deposits has been observed previously by Barbier (22), Van Broekhoven *et al.* (23), and Ostgard *et al.* (9). These researchers have suggested that small platinum particles are less likely to form multiple carbon–metal bonds that are necessary for self-poisoning reactions. In addition, our suggestion that the unique properties of Pt–L-zeolite catalysts for *n*-hexane conversion are due, at least in part, to the stabilization of cluster-sized Pt particles is consistent with the work of Mielczarski *et al.* (24). These authors observed that the catalytic properties of Pt for *n*-hexane conversion were related primarily to the Pt particle size and not to the microstructure of the support.

n-Hexane Reaction Kinetics

It has been suggested that dehydrocyclization reactions over Pt proceed through 1,6- and 1,5-diadsorbed intermediates, which undergo cyclization and dehydrogenation reactions to form benzene and methylcyclopentane (25–27). Branched hexane isomers are formed as secondary products from ring-opening reactions of methylcyclopentane. On platinum, the primary hydrogenolysis reactions of *n*-hexane produce $C_4 + C_2$ and $C_5 + C_1$ hydrocarbons (28). Lighter hydrocarbons, C_1–C_3, are produced mainly from secondary hydrogenolysis reactions. Propane, however, can also be produced as a primary reaction product by the acid-catalyzed conversion of *n*-hexane (13).

The high steady-state dehydrocyclization activity and selectivity of the 1% Pt/K(Ba)–L catalyst is apparent from the results presented in Tables 2 and 3. The ratio of benzene to methylcyclopentane formation rates is equal to 2.3 on the L-zeolite-supported catalyst, indicating that the 1,6-ring closure pathway is more active than 1,5-ring closure. For the 4% Pt/SiO_2 catalyst, however, this ratio is equal to 0.43 at steady-state activity, suggesting that 1,6-ring closure is less active on this catalyst relative to the 1,5-ring closure pathway. The accumulation of carbonaceous species on the silica-supported platinum catalyst, therefore, appears to inhibit the 1,6-cyclization pathway more severely than the 1,5-cyclization pathway. Indeed, Iglesia and Baumgartner (7) have observed that the initial 1,6-ring closure activity for *n*-heptane dehydrocyclization on a clean, silica-supported catalyst is as high as that of the L-zeolite-supported platinum catalyst. Furthermore, the initial activity for 1,6-ring closure over the clean silica-supported catalyst is greater than the initial activity for 1,5-ring closure. These authors also observed the selective decrease in activity for 1,6-ring closure with time on stream for *n*-heptane conversion on silica-supported Pt.

While isomerization of *n*-hexane over platinum can proceed by either a ring-opening or a bond-shift mechanism, the ring-opening pathway generally dominates on clean platinum surfaces (29–31). This behavior is reflected by the observation that the ratio of the rates of formation of methylpentanes to methylcyclopentane is equal to 0.88 for Pt/K(Ba)–L samples. For the aged silica-supported catalyst, however, this ratio is equal to 3.0, which may imply that contributions to the isomer product distribution by the bond-shift pathway may also become important. These results suggest that the ring-opening mechanism may have a stricter site requirement and be more sensitive to surface carbonaceous material than is the bond-shift mechanism.

The hydrogenolysis activities are similar on the Pt/K(Ba)–L and Pt/SiO_2 catalysts, although the L-zeolite-supported catalyst is more selective for terminal cracking as seen by the larger value for the ratio of *n*-pentane and *n*-butane formation rates. Tauster and Steger (16) have attributed this increased terminal cracking tendency of L-zeolite-supported catalysts to geometric effects imposed by the zeolite structure; however, high terminal cracking probability is also observed for clean platinum catalysts (7). While it is possible that the zeolite structure can influence the reaction selectivity, we observe that the hydrogenolysis activation energies for both catalysts are similar, suggesting that similar hydrogenolysis mechanisms may be operative over both catalysts.

It can be seen in Table 4 that the apparent activation energies for benzene and methylcyclopentane formation over the Pt/K(Ba)–L and Pt/SiO_2 catalysts are similar.

This result suggests that similar mechanisms may be involved in the production of these species over both catalysts. As noted earlier, the steady-state rates of benzene and methylcyclopentane formation are an order of magnitude lower over the Pt/SiO_2 catalyst (see Table 3), and the silica-supported platinum catalyst has fewer sites that adsorb carbon monoxide strongly. Thus, the formation of benzene and methylcyclopentane over both catalysts appears to take place by similar mechanisms over both catalysts, with the primary difference between catalysts being that the Pt/SiO_2 catalyst retains fewer strong adsorption sites under steady-state reaction conditions than the Pt/K(Ba)–L catalyst.

We have observed in this study that the hydrogen orders for the hydrogenolysis reactions producing *n*-pentane and *n*-butane are approximately equal to unity, while the hydrogen orders for benzene and methylcyclopentane production are −2.3 and −0.88, respectively.

These results can be reconciled by suggesting that the key surface intermediate in the formation of benzene may be more deeply dehydrogenated than the key intermediate in the formation of methylcyclopentane, and the latter intermediate may be more deeply dehydrogenated than the key intermediates in the formation of hydrogenolysis products. We may assume that a more deeply dehydrogenated surface intermediate forms a larger number of chemical bonds with the platinum surface. Therefore, the rate of benzene formation would be expected to be most sensitive to the presence of coke on the surface, the rate of methylcyclopentane formation would show intermediate sensitivity, while the hydrogenolysis rate would be least sensitive to the presence of coke. This ranking of sensitivity is consistent with the differences in Table 3 between the turnover frequencies over the Pt/K(Ba)–L and Pt/SiO_2 catalysts.

CONCLUSIONS

Results of microcalorimetric and ^{13}C NMR spectroscopic studies of CO adsorption and reaction kinetics measurements indicate that hexane cyclization, aromatization, and isomerization reactions over Pt in L-zeolite and on SiO_2 are similar, and that variations in activity and selectivity are primarily caused by differences in catalyst deactivation. Cluster-sized platinum particles are more resistant to deactivation by self-poisoning reactions than larger platinum particles. Accordingly, the higher steady-state activity of L-zeolite-supported platinum compared to platinum on silica may be attributed to the ability of L-zeolite to stabilize platinum as cluster-sized particles under reforming conditions. The apparent activation energies for dehydrocyclization reactions are essentially the same for both catalysts, suggesting that similar reaction mechanisms are operative over these catalysts. The deactivation of Pt/SiO_2 catalysts for dehydrocyclization reactions can be related to a decrease in the number of sites that adsorb CO strongly, suggesting that these sites are particularly active for dehydrocyclization of *n*-hexane.

ACKNOWLEDGMENTS

We acknowledge the donors of the Petroleum Research Fund, administered by the American Chemical Society, for the partial support of this research. We also acknowledge funding provided by the National Science Foundation. Finally, we thank Randy Cortright for valuable suggestions during the latter stages of this work.

REFERENCES

1. Bernard, J. R., *in* "Proceedings, Fifth International Conference on Zeolites" (L. V. C. Rees, Ed.) p. 686 Heyden, London 1980.
2. Besoukhanova, C., Breysse, M., Bernard, J. R., and Barthomeuf, D., *in* "Stud. Surf. Sci. Catal., Catalyst Deactivation" (B. Delmon and G. F. Froment, Eds.), Vol. 6, p. 201. Elsevier, Amsterdam, 1980.
3. Besoukhanova, C., Breysse, M., Bernard, J. R., and Barthomeuf, D., in "Stud. Surf. Sci. Catal., New Horizons in Catalysis" (T. Seiyama and K. Tanabe, Eds.), Vol 7B, p. 1410. Elsevier, Amsterdam, 1981.
4. Besoukhanova, C., Guidot, J., and Barthomeuf, D., *J. Chem. Soc., Faraday Trans. I* **77,** 1595 (1981).
5. Hughes, T. R., Buss, W. C., Tamm, P. W., and Jacobson, R. L., *in* "Stud. Surf. Sci. and Catal., New Developments in Zeolite Science and Technology," (Y. Murakami, A. Iijima, and J. W. Ward, Eds.), Vol. 28, p. 725. Elsevier, Amsterdam, 1986.
6. Tamm, P. W., Mohr, D. H., and Wilson, C. R., *in* "Stud. Surf. Sci. and Catal., Catalysis, 1987" (J. W. Ward, Ed.), Vol. 38, p. 335. Elsevier, Amsterdam, 1988.
7. Iglesia, E. and Baumgartner, J. E., in "Proceedings, 10th International Congress on Catalysis, Budapest, 1992" (L. Guczi, F. Solymosi, and P. Tétényi, Eds.), p. 157. Akadémiai Kiadó, Budapest, 1993.
8. Sharma, S. B., Miller, J. T., and Dumesic, J. A., *J. Catal.* **148,** 198 (1994).
9. Ostgard, D. J., Kustov, L., Poeppelmeier, K. R., and Sachtler, W. M. H., *J. Catal.* **133,** 342 (1992).
10. Handy, B. H., Sharma, S. B., Spiewak, B. E., and Dumesic, J. A., *Meas. Sci. Technol.* **4,** 1350 (1993).
11. Rivera-Latas, F. J., Dalla Betta, R. A., and Boudart, M., *AIChE J.* **38,** 771 (1992).
12. Sharma, S. B., Laska, T. E., Balaraman, P., Root, T. W., and Dumesic, J. A., submitted for publication.
13. Lane, G. S., Modica, F. S., and Miller, J. T., *J. Catal.* **129,** 145 (1991).
14. Mielczarski, E., Hong, S. B., Davis R. J., and Davis, M. E., *J. Catal.* **134,** 359 (1992).
15. Tauster, S. J. and Steger, J. J., *in* "Mat. Res. Soc. Symp. Proc., Microstructure and Properties of Catalysts" (M. M. J. Treacy, M. M. Thomas, and J. M. White, Eds.), Vol. 111, p. 419. Materials Research Society, Pittsburgh, 1988.
16. Tauster, S. J. and Steger, J. J., *J. Catal.* **125,** 387 (1990).
17. Davis, M. S., Zaera, F., and Somorjai, G. A., *J. Catal.* **85,** 206 (1984).
18. Gates, B. C., "Catalytic Chemistry." Wiley, New York, 1992.

19. Bond, G. C., Cunningham, R. H., and Short, E. L., *in* "Proceedings, 10th International Congress on Catalysis, Budapest, 1992." (L. Guczi, F. Solymosi, and P. Tétényi, Eds.), p. 130. Akadámiai Kiadó, Budapest, 1993.
20. Biswas, J., Bickle, G. M., Gray, P. G., Do, D. D., and Barbier, J., *Catal. Rev. Sci. Eng.* **30,** 161 (1988).
21. Davis, S. M., Zaera, F., and Somorjai, G. A., *J. Catal.* **77,** 439 (1982).
22. Barbier, J., *Appl. Catal.* **23,** 225 (1986).
23. Van Broekhoven, E. H., Schoonhoven, J. W. F. M., and Ponec, V., *Surf. Sci.* **156,** 899 (1985).
24. Mielczarski, E., Hong, S. B., Davis, R. J., and Davis, M. E., *J. Catal.* **134,** 359 (1992).
25. Barron, Y., Cornet, D., Maire, G., and Gault, F. G., *J. Catal.* **2,** 152 (1963).
26. Barron, Y., Maire, G., Muller, J. M., and Gault, F. G., *J. Catal.* **5,** 428 (1966).
27. Dautzenberg, F. M. and Platteeuw, J. C., *J. Catal.* **19,** 41 (1970).
28. Garin, F., Aeiyach, S., Legare, P., and Maire, G., *J. Catal.* **77,** 323 (1982).
29. Corolleur, C., Corolleur, S., and Gault, F. G., *J. Catal.* **24,** 385 (1972).
30. Chambellan, A., Datigues, J.-M., Corolleur, C., and Gault, F. G., *Nouv. J. Chim.* **1,** 41 (1988).
31. Anderson, J. R., *Adv. Catal.* **23,** 1 (1975).